OPEN ACCESS

IR-assisted ionization of helium by attosecond extreme ultraviolet radiation

New Journal of Physics
The open-access journal for physics

IR-assisted ionization of helium by attosecond extreme ultraviolet radiation

P Ranitovic[1,2,5], X M Tong[3,5], B Gramkow[1], S De[1], B DePaola[1], K P Singh[1], W Cao[1], M Magrakvelidze[1], D Ray[1], I Bocharova[1], H Mashiko[1], A Sandhu[4], E Gagnon[4], M M Murnane[4], HC Kapteyn[4], I Litvinyuk[1] and C L Cocke[1,5]

[1] J R Macdonald Lab, Physics Department, Kansas State University, Manhattan, KS 66506, USA

[2] Department of Physics, Stockholm University, AlbaNova University Center, S-10691 Stockholm, Sweden

[3] Institute of Materials Science and Center for Computational Sciences, University of Tsukuba, Tsukuba, Ibaraki 305-8573, Japan

[4] JILA and Department of Physics, University of Colorado and NIST, Boulder, CO 80309-0440, USA

E-mail: predragr@jila.colorado.edu, tong@ims.tsukuba.ac.jp and cocke@phys.ksu.edu

New Journal of Physics **12** (2010) 013008 (12pp)
Received 27 August 2009
Published 15 January 2010
Online at http://www.njp.org/
doi:10.1088/1367-2630/12/1/013008

Abstract. Attosecond science has opened up the possibility of manipulating electrons on their fundamental timescales. Here, we use both theory and experiment to investigate ionization dynamics in helium on the attosecond timescale by simultaneously irradiating the atom with a soft x-ray attosecond pulse train (APT) and an ultrafast laser pulse. Because the APT has resolution in both energy and time, we observe processes that could not be observed without resolution in both domains simultaneously. We show that resonant absorption is important in the excitation of helium and that small changes in energies of harmonics that comprise the APT can result in large changes in the ionization process. With the help of theory, ionization pathways for the infrared-assisted excitation and ionization of helium by extreme ultraviolet (XUV) attosecond pulses have been identified and simple model interpretations have been developed that should be of general applicability to more complex systems (Zewail A 2000 *J. Phys. Chem.* A **104** 5660–94).

[5] Author to whom any correspondence should be addressed.

The use of an attosecond pulse train (APT) is particularly interesting for initiating electronic dynamics in atoms and molecules, because they naturally possess high time and energy resolution, within the limitations of the uncertainty principle. APTs are generated during the process of high-harmonic frequency up-conversion of a femtosecond laser. The resulting extreme ultraviolet (XUV) radiation can span a broad spectrum of harmonics, each with a relatively narrow (i.e. sub-eV) bandwidth. However, the individual harmonic orders are mutually coherent, which in the time domain corresponds to the emission of a series of attosecond bursts. This form of radiation is thus ideally suited for initiating or probing atomic and molecular dynamics in real time, while also retaining spectroscopic selectivity [2]–[6]. Since most dynamic studies use a pump-probe geometry, where one pulse excites a sample and another probes the time evolution, understanding how a simple atomic system, fully accessible to theoretical analysis, responds to attosecond XUV radiation in the presence of a femtosecond laser field is essential for extending the use of attosecond XUV pulses to more complex systems.

Here, we study the infrared (IR)-assisted ionization of He by an APT. A pioneering study of this process was recently carried out by Johnsson *et al* [7], who showed that the probability of ionizing the He by the APT depends on the relative phase of the IR and APT. The interpretation of such an effect is complex, involving consideration of processes such as IR-assisted photoionization/excitation, IR ionization of highly excited states of the He atom and the launching and propagation in the IR field of continuum electron wave packets (EWPs). Only a complete solution to the Schrödinger equation (SE) can take all of these processes into account. Johnsson *et al* [7] carried out such a calculation, for fixed IR and APT wavelengths, and concluded that the major cause of the oscillatory yield was the coherent formation of a train of EWPs launched by the APT into the IR field. A single EWP did not suffice, constructive interference of a series of such packets was found to be necessary. It was concluded in that study that the phase-dependent modulation of the photoionization/photo-excitation probability of individual harmonics by the IR was not an important factor. More recently, Riviere *et al* [8] have analyzed the process using a simple-man model, and used this to predict the outcome of the reaction for different APT/IR parameters.

In this paper, we show that substantial changes in the laser-assisted ionization yield are observed when the frequency of the APT is resonant with one of the He energy levels. We excite specific states of He by employing an APT of sufficient length to retain good spectral resolution. We find that the exact spectral content of the harmonics in the APT plays an important role in determining the ionization pathways. By tuning the wavelength of the harmonics, we can tune into and out of resonance with highly excited states of He. This is most easily observed (experimentally) when the role of IR is to ionize excited states of the He (IR comes after APT, see [6]) but is observed also to be important (theoretically) when the IR and APT are simultaneously present. Even a very weak IR field dramatically modifies the resonances and thus the way in which the He reacts to the APT. To some extent, the IR can be used to control and tune the interaction of the target with the XUV radiation. Full understanding of the cooperative XUV/IR ionization process will be possible without taking this into account.

Attosecond pulses have been successfully produced in the XUV region of the spectrum either as isolated, single-cycle pulses [9]–[11] or as APTs [12]–[15]. The choice of which one of these attosecond fields is appropriate depends on whether temporal or spectral resolution or both are required by a particular application. Figure 1(a) plots a single, 300-attosecond-long XUV pulse, and two pulse trains with different pulse envelopes, composed of a sequence of 300-attosecond-long pulses. Figure 1(b) shows the frequency domain spectra corresponding to

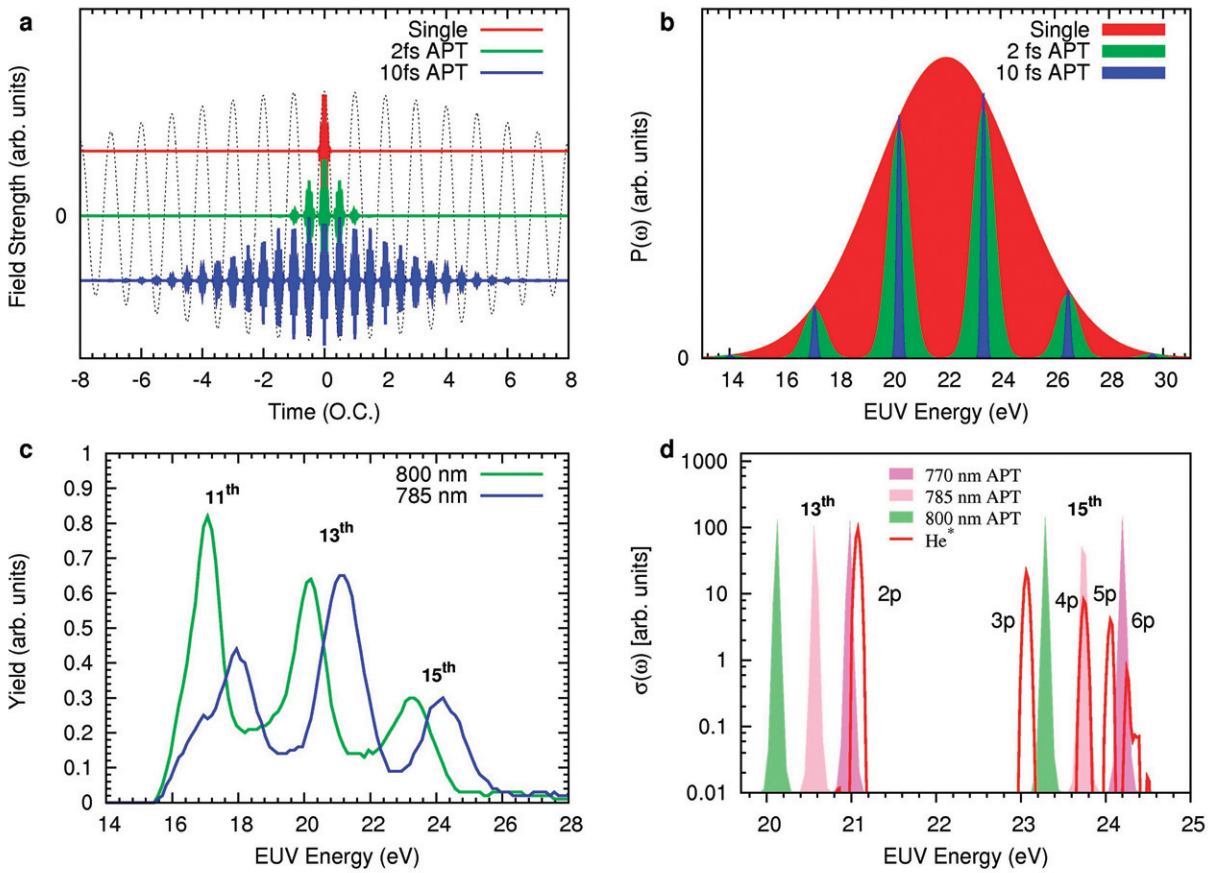

Figure 1. (a) 300 as long XUV pulses in the form of 2 and 10 fs long APTs, and a single, isolated attosecond pulse are presented in green, blue and red, respectively. The dashed line represents a 30 fs long IR pulse. All the pulse durations are considered to be FWHM. (b) The power spectra of the three attosecond pulse forms of (a). The FWHMs in the energy domain are 6, 0.9 and 0.183 eV. The energy resolution of the higher harmonics of the XUV beam is related to the APT duration as $\Delta\omega = 4\ln 2/\tau$, where $\Delta\omega$ represents the FWHM of the harmonics in the frequency domain, and τ stands for the APT duration. (c) The photoelectron energies of Ar correspond to the 11th, 13th and 15th harmonics produced by two different driving IR lasers. The harmonic generation process is optimized in such a way as to minimize the amplitude of the 17th harmonic, which can directly photoionize He. The harmonics driven by the 785 nm show a blue-shift in energy and correspond to the 770 (5) nm fundamental wavelength, while the 800 nm ones exhibit no shift in energy. (d) Calculated excited states of He and the harmonic energies produced by three different IR wavelengths. In the case of 800 nm APT, the energy resolution of the 15th harmonic should be less than 0.7 eV in order to nestle between the 1s3p and 1s4p resonances.

the three time-domain waveforms of figure 1(a). In the case of an isolated attosecond pulse, although the temporal resolution is excellent, the energy uncertainty becomes large and thus isolated attosecond pulses are ideal for use when the coherent excitation of state(s) spanning a

large bandwidth is required. On the other hand, in the case of an APT consisting of many pulses (long envelope), the narrower spectral structure in the XUV harmonics can excite specific states while maintaining very good time resolution.

The experimental set-up uses a cold target recoil-ion momentum spectroscopy (COLTRIMS) geometry where two time- and position-sensitive detectors help us to collect all the reaction products (electrons/ions) in coincidence, and reconstruct their full three-dimensional (3D) momenta. The XUV arm of the interferometer uses a gas-filled hollow-core fiber to efficiently up-convert the driving IR field into an XUV beam, whose higher harmonics can be tuned in the frequency domain. The XUV/IR pulses are made to spatially and temporally overlap on the recombination mirror with a hole, allowing both beams to travel collinearly. The beams from both interferometer arms are focused into a gaseous jet by being reflected off a torroidal mirror. In the first set of experiments, the XUV beam is used to excite a certain Rydberg state of an He atom and is considered as a pump. The IR beam is used as probing, and it is delayed in time relative to the XUV beam. The time delays of the probing IR beam range from attoseconds to picoseconds. In the second set of experiments, we attenuate the IR pulse used to drive the harmonic generation process and let it propagate together with the XUV pulse. The attenuated driving-IR and XUV pulses are locked in phase and overlap temporally. The probing-IR beam in this case is still relatively delayed due to the combination of the driving-IR and XUV pulses. For more details and a picture of the set-up, see the supplementary material (available from stacks.iop.org/NJP/12/013008/mmedia).

We measure the relevant harmonic energies in our XUV beams by photoelectron spectroscopy of Ar. Figure 1(c) shows the energy spectra of photoelectrons ionized from Ar by our XUV APTs. The Ar ionization potential was added to retrieve the harmonic energies. These APTs were generated by exposing a xenon gas to IR of two different central wavelengths, namely 800 (5) and 785 (5) nm. Figure 1(d) shows the spectral overlap of the three groups of the 13th and 15th harmonic pairs with the excited states of He. Throughout the article, the higher harmonics of the 800, 785 and 770 nm fundamental wavelengths will be used to demonstrate the importance of resonant excitation processes in the presence of IR fields. Four methods can, in principle, be used to modify the overlap of the harmonics with the resonances: firstly, by changing the APT duration we can choose the energy resolution of the harmonics (figure 1(b)); secondly, by changing the fundamental wavelength of the driving laser field, we tune the energies of the harmonics; thirdly, by generating the XUV beams in gas-filled hollow-core fibers [16,17], we can fine-tune the XUV photon energies outside of the driving-IR higher-harmonic range (figure 1(c)); finally, by applying an IR field to the atom, we can modify the resonances and change the absorption cross-section of the harmonics at play. An example of the harmonic fine-tuning is shown in figure 1(c), where the measured photoelectron energies exhibit a slight blue-shift from the harmonic energies as being generated by the 785 nm driving IR. The blue-shift in this case corresponds to the effective IR driving wavelength of 770 (5) nm. Whereas the harmonic central energies were measured by the photoelectron spectroscopy of Ar, the energy bandwidth of each harmonic was measured using a spectrometer. Although we have not explicitly characterized the length of our APT, on the basis of the measured spectral resolution we find that the train is typically at least 4 fs long (the spectral resolution of each harmonic measured by the spectrometer was less than 0.5 eV).

It is important to the overall picture of the process at hand to discuss both situations in which the APT and IR act simultaneously and those where they act sequentially. We show in figure 2 our observed He^+ yield as a function of the relative IR/APT delay, with both

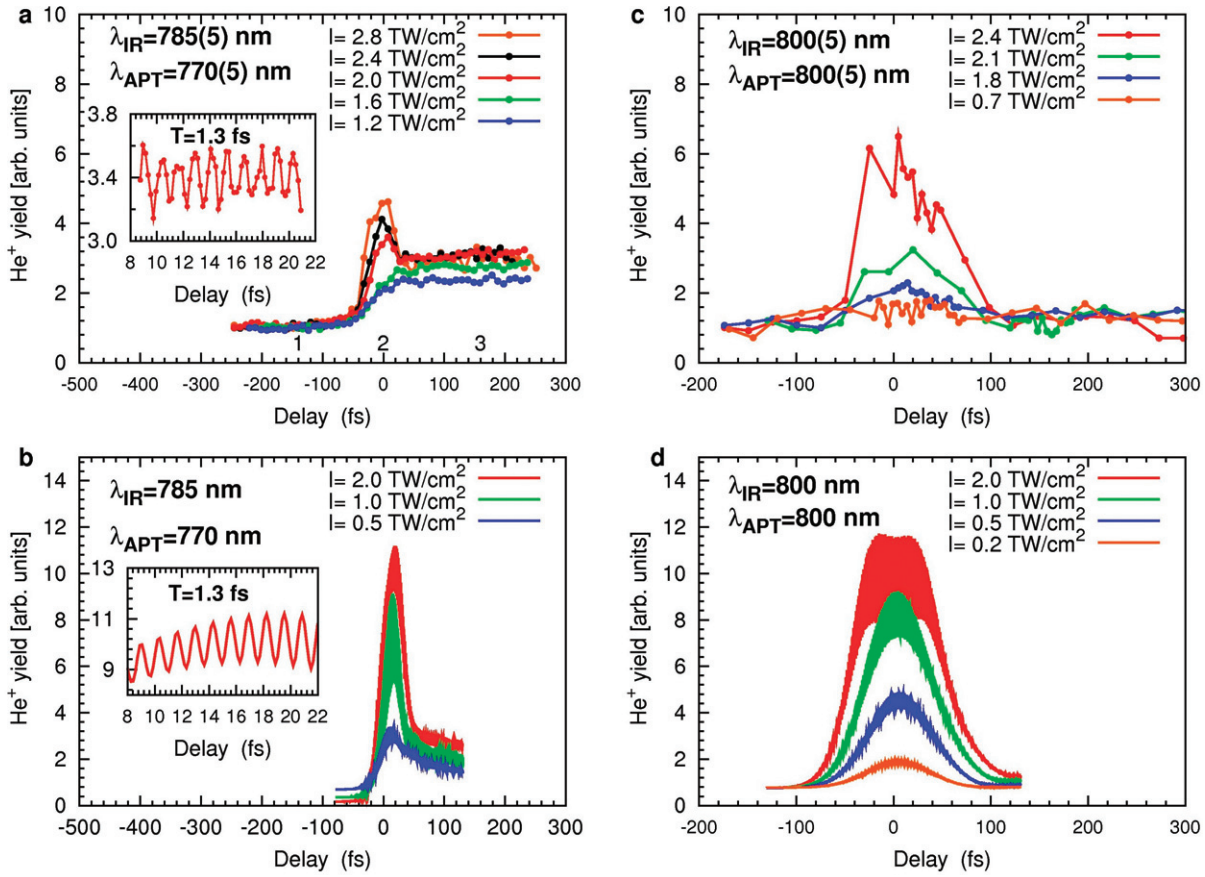

Figure 2. (a) Experimental He^+ yield for five different IR probe intensities at a driving IR wavelength of 785 (5) nm and a pulse duration of 45 fs. The inset shows the modulation of He^+ yield in the overlap region (from 8 to 22 fs IR delays—with an arbitrary absolute zero) with 1.3 fs periodicity and an IR intensity of 2 TW cm^{-2}. (b) Calculated He^+ yields for 0.5, 1 and 2 TW cm^{-2} IR intensities, 785 nm IR wavelength, 770 nm APT and 45 fs IR pulse duration. The inset shows the modulated He^+ yield in the overlap region for the delays from 8 to 22 fs. For the highest IR intensity shown (red), the yield oscillates with a half-an-optical-cycle periodicity (1.3 fs) and exhibits the maximum yield at +20 fs delays. (c) Experimental He^+ yield for four IR intensities, and 800 (5) nm IR and APT wavelengths. (d) Theoretical calculations of the He^+ yield for the 800 nm driving IR wavelength and four IR intensities, calculated for the 80 fs IR pulse duration. The APTs used in the calculations are 10 fs long with the duration of the individual pulses in the train of 300 as.

cycle-averaged and sub-optical-cycle (inset of figure 2(a)) time resolution. For a 45 fs long IR pulse (full-width at half-maximum (FWHM)), the time spectrum can be divided into three regions of interest: (i) when the probing IR pulse arrives before the APT; (ii) when the two pulses overlap in time; and (iii) when the IR pulse ionizes the excited states of He long after the APT is gone. Those three regions are, respectively, marked as 1, 2 and 3 in figure 2(a). If the 15th harmonic (and perhaps 13th) is not resonant with He, we expect the yields in regions

3 and 1 to be the same. In this case, the yields are due to the direct photo-ionization of He by the 17th harmonic. On the other hand, if the APT is tuned to resonantly excite He, the excited states are easily ionized by the IR and the yield in region 3 exceeds that in region 1. This result is seen by comparing the yields in region 3 in figures 2(a) and (c). The enhanced yield in region 3 in figure 2(a) is attributed mainly to resonant excitation of the 5p–6p states in He^* for the shorter wavelength driving IR and blue-shifted harmonics. For the longer wavelength driver (figure 2(c)), the 15th harmonic energy is too low to reach even the 4p resonance. The excited np ($n > 2$) states of He slowly radiatively decay and can be ionized by the IR pulse long after the XUV pulse is gone. We note that on the as–fs–ps timescale probed by this experiment, the nanosecond radiative decay of the excited states is negligible. We also note that the IR probe intensities are not high enough to ionize He without overlapping in time with the XUV pulse.

In order to investigate this behavior more deeply, we have performed a theoretical study of this system by solving the time-dependent SE in the integral form, factoring out the background to improve the numerical precision [18]. The time propagation is performed in a generalized pseudospectral method with a second-order split-operator method [19] in a finite space. This finite space is further divided into two regions: an inner region and an outer region. Once the electron moves into the outer region, we project it on to a Volkov state. The Volkov state is propagated in the momentum space so we remove the space boundary effect [20]. EWPs moving into the outer region at different times will coherently add up. In this way, we can propagate the wavefunction on a very long timescale without worrying about the boundary effect. We obtain all the dynamic information when the time-dependent field is gone.

The theory (figures 2(b)–(d)) for two different driving APT and IR wavelengths confirms that the yield in region 3 strongly depends on whether the XUV beam is resonant with He. The theoretical intensities used do not exactly match the experimental ones. However, the experimental numbers bear large uncertainties (about 50%) due to the difficulty in evaluating exactly the IR field strength at the location of the XUV beam (beam overlap).

In the more complex overlap region, region 2, both the experiment and the theory (figures 2(a) and (b), insets) show that He^+ yield oscillates with a half-an-optical-cycle periodicity of the IR field when the APT and the probing IR pulses are relatively delayed with a sub-optical-cycle resolution, a result in agreement with that of Johnsson *et al* [7]. Both the theory and the experiment show that the He^+ yield strongly depends on the probe IR intensity. We note that the He^+ yield can be altered by 50% in the overlap region by changing the IR intensity by a factor of 2. Such an enhancement was seen and calculated in [7, 8]. Armed with our observation of the importance of the resonant absorption of the 15th harmonic, we suggest an additional mechanism that may contribute to the yield enhancement in region 2: that the presence of the IR field at the moment of excitation by the APT can modify the propensity of the He neutral to absorb the XUV radiation by shifting and broadening the resonances in the atom. The role of resonant absorption in the He neutral is not explicitly mentioned in either [7] or [8].

A simple qualitative discussion of the IR tuning of resonant absorption of the XUV can be developed in a quasi-static picture. If one applies a strong dc electrical field to one of the resonances in He, it develops a width (and shift) due to tunnel ionization; this width is a simple function of the instantaneous field strength. If this field strength is now varied sinusoidally in time, this width will also vary, provided that the characteristic electron motion is faster than the time variation of the IR field. For the case of the 2p resonance, such a picture is perhaps justified, since the Kepler orbit time (1.2 fs) for this state is shorter than the period of the IR field (2.7 fs); for higher np resonances, this condition is not met, and one cannot expect a

discussion based on this picture to have quantitative validity. Indeed, above $n = 3$, an IR field, peak intensity of 10^{12} W cm^{-2}, places the resonances over the barrier. Nevertheless, it is well known that the IR substantially modifies the absorption probability from its normal resonant structure to a completely different structure in which the same absorption strength is distributed over a broad range of frequencies (see below), as would result from the quasi-static picture. We continue a qualitative discussion within the framework of the quasi-static picture only for convenience and not because we intend it to be exact. We point out that the comparison between our experiment and the calculations is in no way dependent on this qualitative picture.

From the quasi-static picture one would expect an enhancement of the He^+ yield in region 2 from the change in the absorption cross-section of the 13th harmonic as the 2p resonance is broadened by the IR into resonance with this harmonic. Such an enhancement would oscillate with a periodicity of one half the optical cycle, since the broadening is sensitive only to the strength and not the sign of the instantaneous IR field. It is quite intuitive to imagine that a slight change in the energy of the 13th harmonic would change its overlap with the broadening resonance and, consequently, the amplitude of the oscillation for the same IR intensity and the same APT duration would be very sensitive to the energy of this harmonic. Another interesting consequence of this model is that it predicts that the use of a single attosecond pulse (SAP) to excite an He atom, instead of an APT (figure 1(b)), should result in a smaller enhancement of the ionization in region 2, since the broad bandwidth of the SAP would average over many resonances and be relatively insensitive to their actual location and widths. In the case where the 13th harmonic is not resonant with the field-free He excited states but the 15th is resonant (figure 2(a)), the IR field could also decrease the average XUV absorption cross-section by broadening the 4p resonance so as to decrease its overlap with the 15th harmonic. The two lowest intensities in that figure show a slight decrease in region 2 relative to region 3, which could be due to this.

In the second phase of this experiment, we introduce a second IR pulse, in addition to the probing IR pulse, in order to better control the amplitude of the IR field and the amplitude of the He^+ yield on sub-optical-cycle timescale. The second IR pulse constitutes a fraction of the light that drives the high harmonic generation (HHG) process and travels collinearly with it. Thus, it carries information about the relative phase of the driving IR pulse and the APT. The experimental results and the corresponding theory are shown in figure 3. By adding a driving IR pulse with an intensity that is only 4% of the probe IR intensity, the resulting IR field strength can be modulated by 20% and the resulting intensity of the total IR field changed by a factor of 2.25 as the phase of the driving and the probing IR pulses is scanned. As would be expected from the data shown in region 2 of figure 2(a), the oscillating intensity of the IR field gives rise to a large oscillating enhancement of the He^+ yield. This yield enhancement is in good agreement with the theoretical one, as shown in figures 3(a) and (c). In general, the yield now shows a full optical cycle periodicity in the overlap region (inset of figures 3(a) and (c)), as expected, since this is the periodicity of the magnitude of the IR field (in this figure, we make a distinction between the central wavelength λ_{IR} of the IR (785 (5) nm) and the effective central wavelength λ_{APT} of the 15th harmonic (770 (5) nm). The latter wavelength is deduced from the observed energies of the photoelectrons. We note that the measured periodicity of the He^+ yield varies from the expected 2.6 to 3 fs during the 40 fs scan in the overlap region (see supplementary figure 2(a) available from stacks.iop.org/NJP/12/013008/mmedia). The slow variation in the period of the oscillation is artificial, and was introduced by the temperature change of the environment, making the XUV/IR interferometer shrink and expand on the nanometer scale, while the delays were kept locked to 150 as steps.

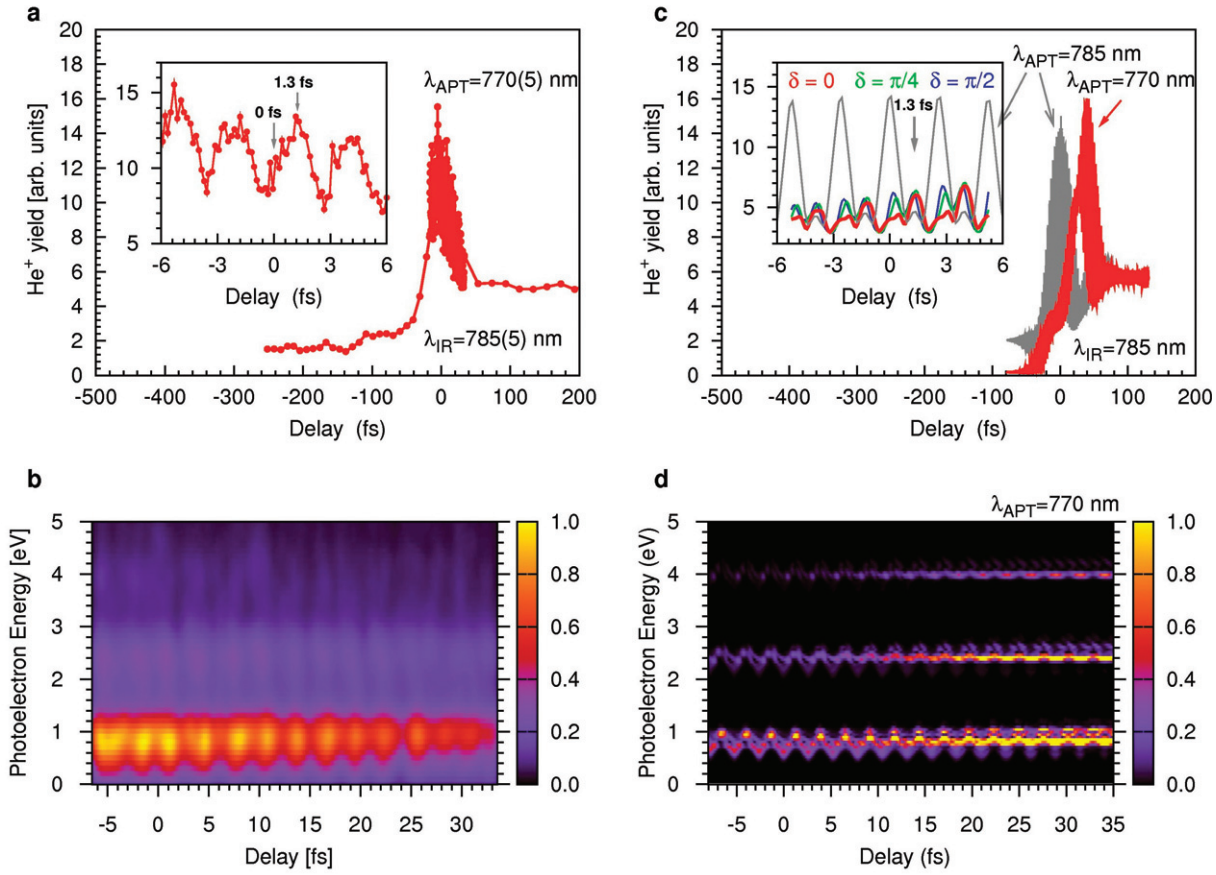

Figure 3. (a) Experimental He^+ yields for 785 (5) nm IR wavelength, a probe IR intensity of 5 TW cm^{-2}, a driving IR intensity of 0.2 TW cm^{-2}, 45 fs IR pulse duration, and the blue-shifted harmonic energies as being generated by 770 (5) nm IR wavelength. The inset shows a zoom into the ± 6 fs delay region, set around arbitrary absolute zero delay. The amplitude of the oscillation starts with 50% modulation. (b) The photoelectrons taken in coincidence with the He^+ ions shown from -7 to 35 fs IR probe delays. (c) Theoretical calculations of the He^+ yield performed with the given experimental IR intensity parameters, 785 nm IR wavelengths, 45 fs long IR pulses and the APT wavelength of 770 and 785 nm. The APT is 10 fs long with 300 as long individual attosecond pulses in the pulse train. The inset shows the yields from ± 6 fs delays for three different phases of the 770 nm APT and the driving IR pulses. For $\delta = 0$, the APT train is locked to the maximum of the driving IR pulse. At zero delay, the probe and driving IR pulses interfere constructively. For $\delta = \pi/4$ and $\delta = \pi/2$, the APT is locked to the driving IR pulse with the 1/8 and 1/4 optical cycle shifts from the maximum driving IR field, respectively. For the 785 nm APT, the phase in between the driving and the probing IR pulses is $\delta = 0$. We note that due to the comparison with the experiment, the theoretical yields for the 770 nm APT were divided by a factor of 3 compared to the 785 nm APT case. (d) Calculated photoelectron distributions corresponding to the ion yields of region 2 of figure 3(c), $\delta = 0$ and 770 nm APT.

Through the theoretical calculations shown in figure 3(c), we illustrate the extreme sensitivity of the yield profile to the energy of the harmonics, an effect we attribute to the roles played by the resonances in He. The red and gray curves correspond to λ_{APT} values of 770 and 785 nm, respectively, and the results are quite different. For the 770 nm case, the 15th harmonic is resonant with the 6p state; for the 785 nm case, it is resonant with the 4p state. The resulting effect on the He^+ yield is dramatic and too complex to be amenable to a simplistic explanation (compare the detail shown in the inset of figure 3(c) and that in the supplementary material available from stacks.iop.org/NJP/12/013008/mmedia), even shifting the time dependence of the yield enhancement. Based on the measured experimental uncertainties and the unknown phase of the driving IR and the APT fields, it is not surprising that no exact agreement between experiment and theory in figures 3(a) and (c) is seen.

Expanded views of the photoelectron energies in the overlap region 2 are shown in figures 3(b) and (d). Examining first the theoretical spectrum, we observe qualitative differences between long delays where the IR comes mainly after the APT (region 3; delays 30–35 fs) and short delays where the two fields strongly overlap (region 2; delays 0–10 fs). In region 2, the energy spectrum is much broader and does not reflect the resonant structure of the He but the energy distribution of the driving harmonic. For example, if the 15th harmonic was dominant, with an energy of 24.2 eV, the population of excited states of He at this energy followed by single photon absorption from the IR would produce photoelectrons of 1.17 eV minus the ponderomotive energy (U_p) of the IR field. When driving and probing IR fields are added coherently, a single IR field results for each value of the APT/probing-IR delay. As this delay is varied, the strength of this field is rapidly and markedly varied, as is the ponderomotive energy. For the IR intensities used in the experiment, the ponderomotive energy is expected to swing between 414 and 184 meV (7.2–3.2 TW cm^{-2}) as the relative delay of the two IR fields is varied between constructive and destructive interference. Thus, a broad band of photoelectron energies reflecting the width of the 15th harmonic, swinging between approximately 756 and 986 meV due to the swing of the ponderomotive energy, is seen. In region 3, however, sharper energy features appear at 35 fs delays, which can be attributed to the smaller ponderomotive shift of the ionization potential. For even longer delays, when the two IR pulses do not temporally overlap anymore, these features become very sharp because they represent a few-photon ionization of well-defined eigenstates of the energy in He. For the two APT wavelengths shown in figure 3(c) (region 3), the resonant excitation of the He 4p and 6p states is modified by the driving-IR pulse. These general features, evolution from broad features in region 2 to sharp ones in region 3, are consistent throughout the theoretical calculations (see the supplementary material available from stacks.iop.org/NJP/12/013008/mmedia). By comparing the photoelectron distributions near zero delay with those near a delay of 35 fs, we see also that the yield of ionization decreases. We interpret this as largely due to the loss of resonant absorption of the He excited states and the XUV harmonics.

The discussion above suggests that the resonance of the 15th harmonic with the 4p and 6p states of He dominates the ionization process in region 3, while the non-resonant 13th harmonic can be put into action by the IR field in the overlap region. We can probe this issue further by examining the photoelectron angular distributions. We first address this through the theoretical spectra, which have better resolution. Figures 4(a) and (b) show the theoretical photoelectron momentum distributions at the maximum and minimum of the IR field, respectively. We focus our discussion on the lowest momentum ring with a radius near 0.2 a.u. (corresponding to the lowest energy line in figure 3(d)). If this photoelectron were ejected by absorption of the 15th

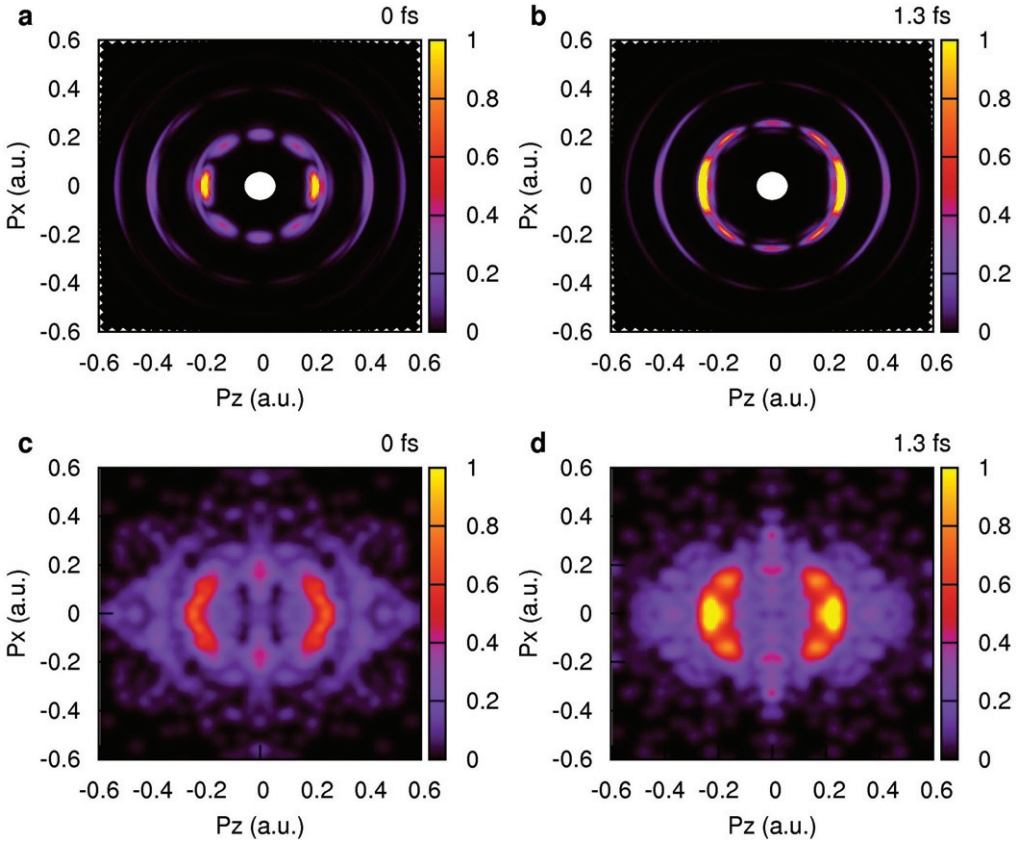

Figure 4. (a) Photoelectron momentum distributions corresponding to the data of figure 3(d), zero delay and $\delta = 0$. (b) Photoelectron momentum distributions corresponding to the data of figure 3(d), and 1.3 fs IR delay. (c) Experimental photoelectron momenta corresponding to zero delay as shown in figures 3(a) and (b). (d) Experimental momenta distributions for the IR probe delayed by 1.3 fs, as shown in figures 3(a) and (b).

harmonic, followed by a single IR photon, the expected angular distribution should have at most a d-wave structure with two angular nodes for positive p_x. The calculations shown in figures 4(a) and (b) show clear evidence for g-waves, requiring the absorption of at least four photons. The 13th-harmonic-plus-3 IR-photons channel could produce such angular structure. This behavior suggests that the 13th harmonic participates strongly in the initial excitation step. This result is not surprising, as can be seen from figure 1(d), which shows that the absorption cross-section of the 2p resonance differs by two orders of magnitude compared with the 6p state. Thus, the probability of absorbing three IR photons by the excitation region populated by the 13th harmonic can compete with the single absorption of an IR photon by the region populated by the 15th harmonic, and the angular distributions, showing the mixes of d- and g-waves, indicate that this is the case. Figures 4(c) and (d) show the experimental angular distributions corresponding to the theoretical ones of figures 4(a) and (b). The momenta correspond to the ion yields as marked with arrows in the inset of figure 3(a). The g-wave patterns are supported by the data, although the statistical errors in the data preclude a definite identification of this, as do the theoretical ones. The second photoelectron band shown in figure 4(a) reveals an h-wave pattern with five nodes in the positive p_x direction. In this multi-color, multi-photon picture, the h-wave

angular pattern would correspond to the five-photon-absorption channel (13th harmonic +4 IR photons). Here, we note that the theoretical XUV beam has a small contribution of the 17th harmonic (figure 1(b)), which can contribute to the photoelectron yield of the second band too.

It is probable that both the resonance-broadening picture and the picture of interfering wavepackets are important in understanding this problem. We suggest that experiments in which the spectral content of the APT is carefully controlled and probably limited to either one or two harmonics could lead to a better understanding of this situation. For example, one harmonic could be spectrally selected from the APT (either 13th or 15th) and the experiment repeated. Should the oscillatory yield persist in such a case, it would provide further evidence of the resonance-broadening effect.

In conclusion, we have shown that the major features of the ionization of He by the coupled action of an APT and an IR field are extremely sensitive to the spectral as well as the time content of the APT. When atomic systems with resonant structures are probed in the presence of strong fields, the resonant structures still play an important role. The experimental data presented here show this for the case where the APT precedes the IR. Since the APT probes an isolated atom, the importance of the resonance is clear. However, the calculations show that this is also true in region 2 where the APT and IR are present simultaneously. Indeed, the results of the calculations in this region are quite sensitive to all parameters, including length of the APT, central wavelength of the APT, and phase of the IR relative to the APT.

In the two-IR case, where one of the composite IR components is locked in phase to the APT by the physics of the capillary, the results of the calculations are even sensitive to the value to which this phase is locked. For example, in the inset of figure 3(c) the micro-structures of the oscillations in region 2 show very different structures depending on the assumed relative phase between the APT and the pump IR. If compared with the one-IR case (inset of figure 2(a)), the fine structure seen in the inset of figure 3(a) tells us that we are not seeing the experimental noise. We do not probe this issue further in this paper experimentally, but it is clear that refinement of the data to probe this question would reveal further details of this effect. We believe that sensitivity to the resonant structure of the target will be a general feature of IR-assisted ionization of atomic and molecular systems by XUV radiation.

Acknowledgments

We thank Gerhard Paulus, Brett Esry, A T Lee and C D Lin for useful discussions. The numerical calculations were carried out by the T2K-Tsukuba System at the Center for Computational Sciences, University of Tsukuba. XMT was supported by Grants-in-Aid for Scientific Research (C) from the Japan Society for the Promotion of Science. PR thanks Jarlath McKenna and Steve Gilbertson for their support during the data-taking process. This work was supported by the Chemical Sciences, Geosciences and Biosciences Division, Office of Basic Energy Sciences, the US Army Research Office, under grant number W911NF-07-1-0475; the US Department of Energy; and NSF grant number 0822646.

References

[1] Zewail A 2000 Femtochemistry: atomic-scale dynamics of the chemical bond *J. Phys. Chem.* A **104** 5660–94 (adapted from the Nobel Lecture)

[2] Drescher M *et al* 2002 Time-resolved atomic inner-shell spectroscopy *Nature* **419** 803–7

[3] Kienberger R *et al* 2004 Atomic transient recorder *Nature* **427** 817–21

[4] Lopez-Martens R *et al* 2005 Amplitude and phase control of attosecond light pulses *Phys. Rev. Lett.* **94** 033001
[5] Goulielmakis E *et al* 2004 Direct measurement of light waves *Science* **305** 1267–9
[6] Haber L H, Doughty B and Leone S R 2009 Continuum phase shifts and partial cross sections for photoionization from excited states of atomic helium measured by high-order harmonic optical pump-probe velocity map imaging *Phys. Rev.* A **79** 031401
[7] Johnsson P *et al* 2007 Attosecond control of ionization by wave-packet interference *Phys. Rev. Lett.* **99** 233001
[8] Riviére P, Uhden O, Saalmann U and Rost J M 2009 Strong field dynamics with ultrashort electron wave packet replicas *New J. Phys.* **11** 053011
[9] Hentschel M *et al* 2001 Attosecond metrology *Nature* **414** 509–13
[10] Sansone G *et al* 2006 Isolated single-cycle attosecond pulses *Science* **314** 443–6
[11] Goulielmakis E *et al* 2008 Single-cycle nonlinear optics *Science* **320** 1614–7
[12] Paul P M *et al* 2001 Observation of a train of attosecond pulses from high harmonic generation *Science* **292** 1689
[13] Mairesse Y *et al* 2003 Attosecond synchronization of high-harmonic soft x-rays *Science* **302** 1540
[14] Tzallas P *et al* 2003 Direct observation of attosecond light bunching *Nature* **426** 267–71
[15] Mauritsson J *et al* 2006 Attosecond pulse trains generated using two color laser fields *Phys. Rev. Lett.* **97** 013001
[16] Rundquist A *et al* 1998 Phase-matched generation of coherent soft x-rays *Science* **280** 1412–5
[17] Sandhu A S *et al* 2006 Generation of sub-optical-cycle, carrier-envelope-phase-insensitive, extreme-UV pulses via nonlinear stabilization in a waveguide *Phys. Rev.* A **74** 061803
[18] Tong X M, Watahiki S, Hino K, and and Toshima N 2007 Numerical observation of the rescattering wavepacket in laser–atom interactions *Phys. Rev. Lett.* **99** 093001
[19] Tong X M and Chu S I 1997 Theoretical study of multiple high-order harmonic generation by intense ultrashort pulsed laser fields: a new generalized pseudo-spectral time-dependent method *Chem. Phys.* **217** 119–30
[20] Tong X M, Hino K, and and Toshima N 2006 Phase-dependent atomic ionization in few-cycle intense laser fields *Phys. Rev.* A **74** 031405